FEBS Letters 553 (2003) 232–238 FEBS 27654

Solution structure of epiregulin and the effect of its C-terminal domain for receptor binding affinity

Katsuharu Sato[a], Takashi Nakamura[a], Mineyuki Mizuguchi[a], Kazunori Miura[a,b], Masahito Tada[a], Tomoyasu Aizawa[a,b], Tomoharu Gomi[c], Kaoru Miyamoto[d,e], Keiichi Kawano[a,*]

[a] *Faculty of Pharmaceutical Sciences, Toyama Medical and Pharmaceutical University, 2630 Sugitani, Toyama 930-0194, Japan*
[b] *Bio-oriented Technology Research Advancement Institution, Saitama 331-8537, Japan*
[c] *Scientific Instrument Center, Toyama Medical and Pharmaceutical University, 2630 Sugitani, Toyama 930-0194, Japan*
[d] *Department of Biochemistry, Fukui Medical University, Shimoaizuki, Matsuoka, Fukui 910-1193, Japan*
[e] *Core Research for Evolutional Science and Technology, Japan Science and Technology Corporation, Tokyo 101-0062, Japan*

Received 1 August 2003; revised 15 August 2003; accepted 22 August 2003

First published online 18 September 2003

Edited by Thomas L. James

Abstract Epiregulin (EPR), a novel member of epidermal growth factor (EGF) family, is a ligand for ErbB-1 and ErbB-4 receptors. The binding affinity of EPR for the receptors is lower than those of other EGF-family ligands. The solution structure of EPR was determined using two-dimensional nuclear magnetic resonance spectroscopy. The secondary structure in the C-terminal domain of EPR is different from other EGF-family ligands because of the lack of hydrogen bonds. The structural difference in the C-terminal domain may provide an explanation for the reduced binding affinity of EPR to the ErbB receptors.

Key words: Epiregulin; Nuclear magnetic resonance; Epidermal growth factor; Structure

1. Introduction

Epiregulin (EPR) is a novel growth-regulating ligand belonging to the epidermal growth factor (EGF) family, which is purified from conditioned medium of the mouse fibroblast-derived tumor cell line NIH3T3/clone T7 [1,2]. Human EPR is mainly expressed on peripheral blood macrophages, placenta in normal tissues and epithelial tumor cell lines [3]. EPR exhibits bifunctional regulatory properties: it inhibits the growth of some epithelial tumor cells and stimulates the growth of fibroblasts and various other types of cells [1]. EPR stimulates the proliferation of gastric cells [4] and human keratinocytes [5,6], and it is a factor affecting pancreatic cancer and inflammatory disease [7,8]. Therefore, EPR plays a critical role in regulating several biological activities.

EPR consists of 46 amino acid residues, and the amino acid sequence of EPR exhibited 24–50% amino acid sequence identity with sequences of other EGF-family ligands [1]. EGF-family ligands act as a trigger for the signal transmission system by binding to the receptors [9]. These receptors are known as ErbB-family receptors, and they consist of four types: ErbB-1, ErbB-2, ErbB-3 and ErbB-4. EPR binds to ErbB-1 and ErbB-4 [10–12], and its selectivity for ErbB-family receptor is similar to that for betacellulin (BTC).

Jones et al. have reported comparisons of binding specificities and affinities of EGF-family ligands for ErbB receptors [11]. According to their findings, the binding affinities of EGF, transforming growth factor-α (TGF-α), BTC, heparin-binding EGF-like growth factor (HB-EGF), heregulin-α (HRG-α), and -β for each ErbB receptor are high or moderate. On the other hand, binding affinities of EPR for ErbB receptors are weak. EPR shows the weakest affinity for both the homodimer and heterodimer of ErbB receptors.

Among EGF-family ligands, the tertiary structures of EGF [13], TGF-α [14], the EGF-like domain of HRG-α (HRG-αe) [15], the EGF-like domain of BTC (BTCe) [16], and HB-EGF [17] have been determined using nuclear magnetic resonance (NMR) spectroscopy or X-ray diffraction. Despite the primary sequence diversity, these tertiary structures are very similar. All EGF-family ligands are composed of N- and C-terminal domains, each of which has a β-sheet.

The C-terminal domain is suggested to be involved in the binding of EGF-family ligands to ErbB receptor. For example, the substitution of the highly conserved Arg^{41} and Leu^{47} of EGF results in a marked reduction in the affinity for the EGF receptor, suggesting that these residues are essential for binding to the receptors [18,19]. It has been reported that the substitution of the C-terminal tail of human TGF-α into human EGF results in high-affinity binding of human EGF to the chicken ErbB-1 [20].

In this study we examine the structure of EPR by NMR spectroscopy and discuss the relation between the binding affinity and the tertiary structure. The report presented here may provide crucial information for elucidating the detailed

*Corresponding author. Fax: (81)-76-434 5061.
E-mail address: kawano@ms.toyama-mpu.ac.jp (K. Kawano).

Abbreviations: EPR, epiregulin; EGF, epidermal growth factor; BTC, betacellulin; TGF, transforming growth factor; HB-EGF, heparin-binding EGF-like growth factor; HRG, heregulin; HRG-αe, EGF-like domain of HRG-α; BTCe, EGF-like domain of BTC; NMR, nuclear magnetic resonance; Trx, thioredoxin; DQF-COSY, double quantum filtered correlation spectroscopy; TOCSY, total correlation spectroscopy; NOESY, nuclear Overhauser enhancement spectroscopy; NOE, nuclear Overhauser effect; CSI, chemical shift index; SA, simulated annealing; RMSD, root mean square deviation; GBP, growth-blocking peptide

0014-5793/03/$22.00
doi:10.1016/S0014-5793(03)01005-6

mechanisms underlying binding affinity of the EGF-family ligand for ErbB-family receptor.

2. Materials and methods

2.1. Sample preparation of EPR

The DNA fragment encoding EPR was inserted into the expression vector, pET32a (Novagen), and EPR was expressed as a soluble form of thioredoxin (Trx)-His-tag fusion proteins. The Trx-His-tag-fusion EPR was expressed in AD494(DE3), which is a Trx reductase-deficient *Escherichia coli* strain. The soluble fraction was purified by His-tag affinity chromatography using Ni-NTA agarose (Qiagen). The buffer of the protein solution eluted was changed to EKMax reaction buffer (Invitrogen) using a PD-10 column (Amersham Pharmacia Biotech). EKMax (Invitrogen) enzyme was added at a final ratio of 0.5 units per 1 mg of protein and incubated at 33°C for 12 h. Finally, the cleavage products were purified by reverse-phase high-performance liquid chromatography. The purified EPR was identified by mass spectrometry (MALDI-TOF MS: Voyager) and N-terminal amino acid analysis (Shimadzu PPSQ-21). The biological activity of the purified EPR was confirmed by growth inhibitory activity for A431 [1]. A431 cells were plated in 96-well dishes at a density of 1.5×10^3 cells/well in the medium containing 10% fetal bovine serum and incubated at 37°C for 24 h. Then, EPR was added at various concentrations [21]. After 3 days, TetraColor ONE (Seikagaku Corporation), which is a reagent for modified MTT assay, was added to each well, and, after 4 h of incubation, the absorbance at 450 nm was measured.

2.2. ^1H NMR spectroscopy

The EPR sample was dissolved at a final concentration of 1.5 mM in 300 μl of either 90% H_2O/10% D_2O or 100% D_2O. The pH was adjusted to 3.4 to observe amide protons by decreasing the hydrogen–deuterium (H–D) exchange rates. The NMR experiments were performed on a Bruker DMX-500 spectrometer. The majority of NMR spectra were recorded at 30°C, and some experiments were carried out at 40°C to resolve ambiguities. Double quantum filtered correlation spectroscopy (DQF-COSY) [22] spectra were collected at 30°C. Total correlation spectroscopy (TOCSY) [23] spectra were obtained at 30°C and 40°C with a mixing time of 80 ms. Nuclear Overhauser enhancement spectroscopy (NOESY) [24] spectra were collected at 30°C and 40°C with a mixing time of 100 and 150 ms. The TOCSY and NOESY spectra at 30°C and pH 7.0 were measured and the ^1H resonances were partially assigned. However, the quality of NMR spectra at pH 7.0 was not good enough to solve the solution structure of EPR. All NMR data were processed and analyzed on a LINUX workstation using NMRpipe1.8 [25] and PIPP 4.3.2 [26] software.

2.3. Structural calculations

The interproton distance restraints were calibrated using nuclear Overhauser effect (NOE) peak intensities. The ϕ angle restraints were applied using spin–spin coupling constants $^3J_{NH\alpha H}$ and chemical shift index (CSI) [27] analysis data. The $^3J_{NH\alpha H}$ coupling constants were determined from a high digital resolution DQF-COSY spectrum. Residues with $^3J_{NH\alpha H} > 10$ Hz were constrained to $\phi = -120 \pm 40°$. When $^3J_{NH\alpha H}$ was not obtained, the ϕ angle was constricted on the basis of CSI data, i.e. $\phi = -60 \pm 30°$ for the residue with CSI = 1. The Backbone ϕ angle restraints were applied for 33 residues on the basis of $^3J_{NH\alpha H}$ and five residues on the basis of CSI. The backbone amide H–D exchange experiment was performed to identify the hydrogen bond donors forming secondary structures. Residues for which the amide proton exchange rates are sufficiently slow were identified in the NOESY spectrum of a freshly prepared solution of EPR in D_2O. For each donor, its acceptor was determined on the basis of the preliminary calculated structure. The hydrogen-bonding restraints were included only in the regions of identified secondary structure and set to be 2.00 ± 0.20 Å for NH–O distances and 3.00 ± 0.30 Å for N–O distances for regular secondary structures. This information about the hydrogen bonds was used to calculate the tertiary structure. During the initial calculation stage, 50 starting structures were calculated from an extended conformation of EPR using a simulated annealing (SA) protocol in X-PLOR 3.1 [28]. The structural refinement was carried out by starting with the 40 lowest-energy structures of the previous iteration. The energy-minimized average structure of EPR was calculated using the modified SA protocol by starting with the 40 lowest-energy structures of the final iteration. All structural calculations were performed on a LINUX workstation. Validation of the final structures was confirmed using PROCHECK-NMR [38]. Ramachandran plot analysis showed that all of the residues have backbone dihedral angles in the allowed regions of the ϕ, ψ plot. The structures were displayed using MOLMOL [29].

2.4. Comparison with other EGF-family proteins

To compare the structural properties of EPR with those of other EGF-family proteins, we used the coordinate data from the Protein Data Bank (PDB). The secondary and tertiary structures of EPR were compared with those of human TGF-α (the PDB accession code is 2TGF) [14], mouse EGF (1EGF) [13], HRG-αe (1HAF) [15], HB-EGF (1XDT) [17], and human BTCe (1IOX) [16].

2.5. Circular dichroism (CD) spectroscopy

CD spectra of EPR were measured using a JASCO J-805 spectrometer (Japan Spectroscopic Co., Ltd., Tokyo, Japan) with a 1-mm quartz cell. The protein concentrations for CD measurements were 155 μM. Protein concentrations were determined by absorbance measurements at 280 nm. The temperature of the measuring cell was maintained at 25°C by circulating water. Buffer solutions contained 250 mM phosphate (pH 6.0 or 7.0) or 250 mM glycine (pH 3.4).

3. Results and discussion

3.1. Chemical shift assignments of EPR

The chemical shift assignment of EPR was carried out using the sequential assignment procedure [30]. The sequential assignment was achieved by a combination of TOCSY and NOESY spectra acquired at 30°C and 40°C. The ^1H resonance of all of the main chain atoms, except for the amide proton of the N-terminal Val[1], and most of the side chain atoms of EPR at pH 3.4 were unambiguously assigned. The assignment of

Table 1
Structural statistics for the family of 40 structures of EPR

Experimental restraints	
Intraresidue distances ($i-j=0$)	297
Sequential distances ($\|i-j\|=1$)	128
Medium-range distances ($\|i-j\|<=4$)	46
Long-range distances ($\|i-j\|>5$)	85
Hydrogen bonds	9
Dihedral angles	38
Total	603
Mean RMSDs from idealized covalent geometry[a]	
Bonds (Å)	0.002 ± 0.000
Angles (deg)	0.511 ± 0.011
Impropers (deg)	0.361 ± 0.014
Mean X-PLOR energies (kcal mol^{-1})	
E_{NOE}[b]	99.77 ± 2.12
E_{cdih}[b]	0.39 ± 0.09
E_{bond}	2.18 ± 0.39
E_{VDW}	21.78 ± 1.22
Atomic RMSDs (Å)[c]	
Well-defined region (residues 4–44)	
Backbone atoms	0.97 ± 0.25
Heavy atoms	1.51 ± 0.27
N-terminal domain (residues 4–33)	
Backbone atoms	0.90 ± 0.28
Heavy atoms	1.50 ± 0.32
C-terminal domain (residues 34–44)	
Backbone atoms	0.48 ± 0.21
Heavy atoms	0.98 ± 0.26

[a]Idealized geometry is defined by the CHARMM force field as implemented within X-PLOR.
[b]The final values of the square-well NOE and dihedral angle potentials were calculated with force constants of 50 and 200 kcal mol^{-1} $Å^{-2}$, respectively.
[c]Atomic differences are given as the average difference against the mean coordinate structure. All statistics are given as means ± S.D.

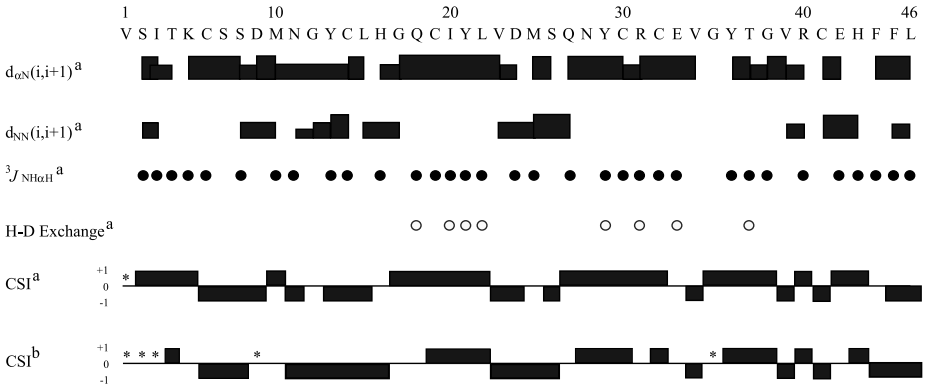

Fig. 1. Diagram of NOE connectivities between protons of neighboring ($d_{\alpha N}$ and d_{NN}), *J*-coupling constants ($^3J_{NH\alpha H}$), slowly exchanging amide protons in D_2O, and CSI analysis [27]. The strength of the observed NOE in NOESY spectra at 30°C is represented by the thickness of the bars. Residues with $^3J_{NH\alpha H} > 10$ Hz are indicated by closed circles. The backbone amide protons, which exchange slowly with D_2O, are indicated by open circles. The bottom plot represents the CSI analysis [27] for the $C_\alpha H$ resonances, where CSI is shown as positive if the $C_\alpha H$ resonance is >0.1 ppm downfield from its random coil value, negative if $0.1 >$ ppm upfield, or 0 if within 0.1 ppm of its random coil value [27]. [a]pH 3.4; [b]pH 7.0; *not determined.

^{1}H resonances of EPR at 30°C and pH 3.4 was deposited in the BioMagResBank (accession number 5173). Fig. 1 summarizes the sequential NOE connectivities, $^3J_{NH\alpha H}$, the slowly exchanging amide protons and the CSI analysis.

3.2. Structural calculation of EPR

The solution structure of EPR at 30°C and pH 3.4 was calculated using NMR-derived 603 experimental restraints. A total of 556 distance restraints were obtained from the NOESY spectrum. The distance restraints can be subdivided into 297 intraresidual, 128 sequential, 46 medium-range, and 85 long-range restraints. The 38 dihedral ϕ angle restraints and nine hydrogen bond restraints were used as additional restraints for the calculations. Fig. 2A shows the ensemble of 40 NMR structures of EPR best fitted for the backbone atoms of the converged region (Thr^4-Phe^{44}). The root mean square deviation (RMSD) of the backbone atoms evaluated for the converged region of the 40 structures against the mean structure was 0.97 ± 0.25 Å for the backbone atoms and 1.51 ± 0.27 Å for all non-hydrogen atoms. The RMSD of the backbone atoms evaluated for the N-terminal (Thr^4-Glu^{33}) and C-terminal (Val^{34}-Phe^{44}) domains are 0.90 ± 0.28 and 0.48 ± 0.21 Å, respectively (Table 1). The RMSD of the β-sheet comprised of strand-2 and -3 in the N-terminal domain (Gly^{17}-Cys^{32}) is 0.37 ± 0.11 Å.

Fig. 2B shows a ribbon drawing of the energy-minimized average structure of EPR. Secondary structures were determined using the program MOLMOL [29]. EPR is comprised of three strands (strand-1, -2, and -3 are composed of Thr^4-Lys^5, Gly^{17}-Leu^{22}, and Gln^{27}-Cys^{32}, respectively) and one

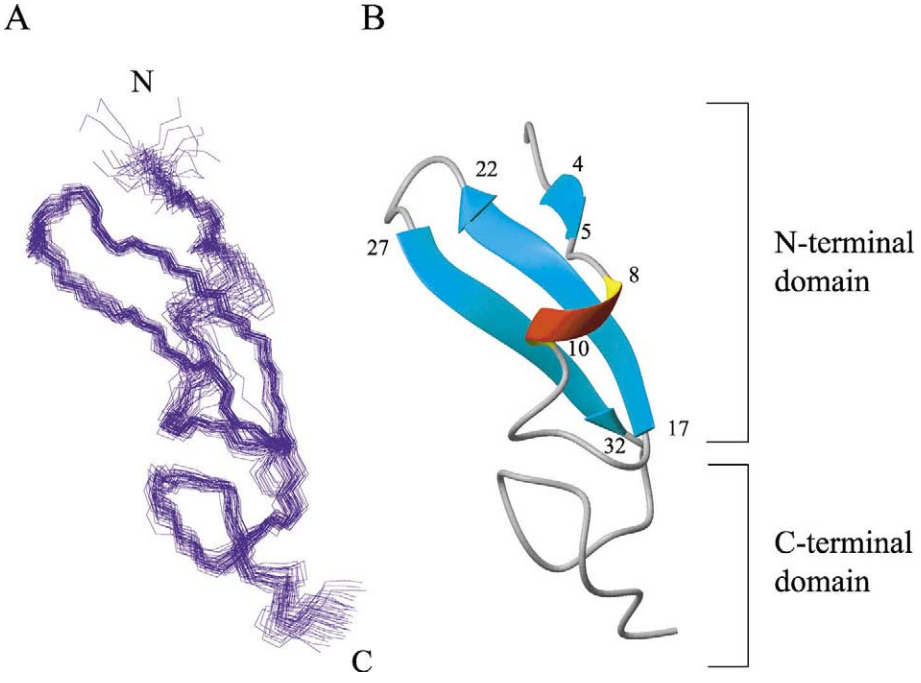

Fig. 2. Tertiary structure of EPR. A: The ensemble of 40 NMR structures of EPR superimposed and fitted for the backbone atoms of residues 4–44. B: The ribbon drawing of the minimized average structure of EPR. Sequence numbers of some residues are indicated. These diagrams were generated using the program MOLMOL [30].

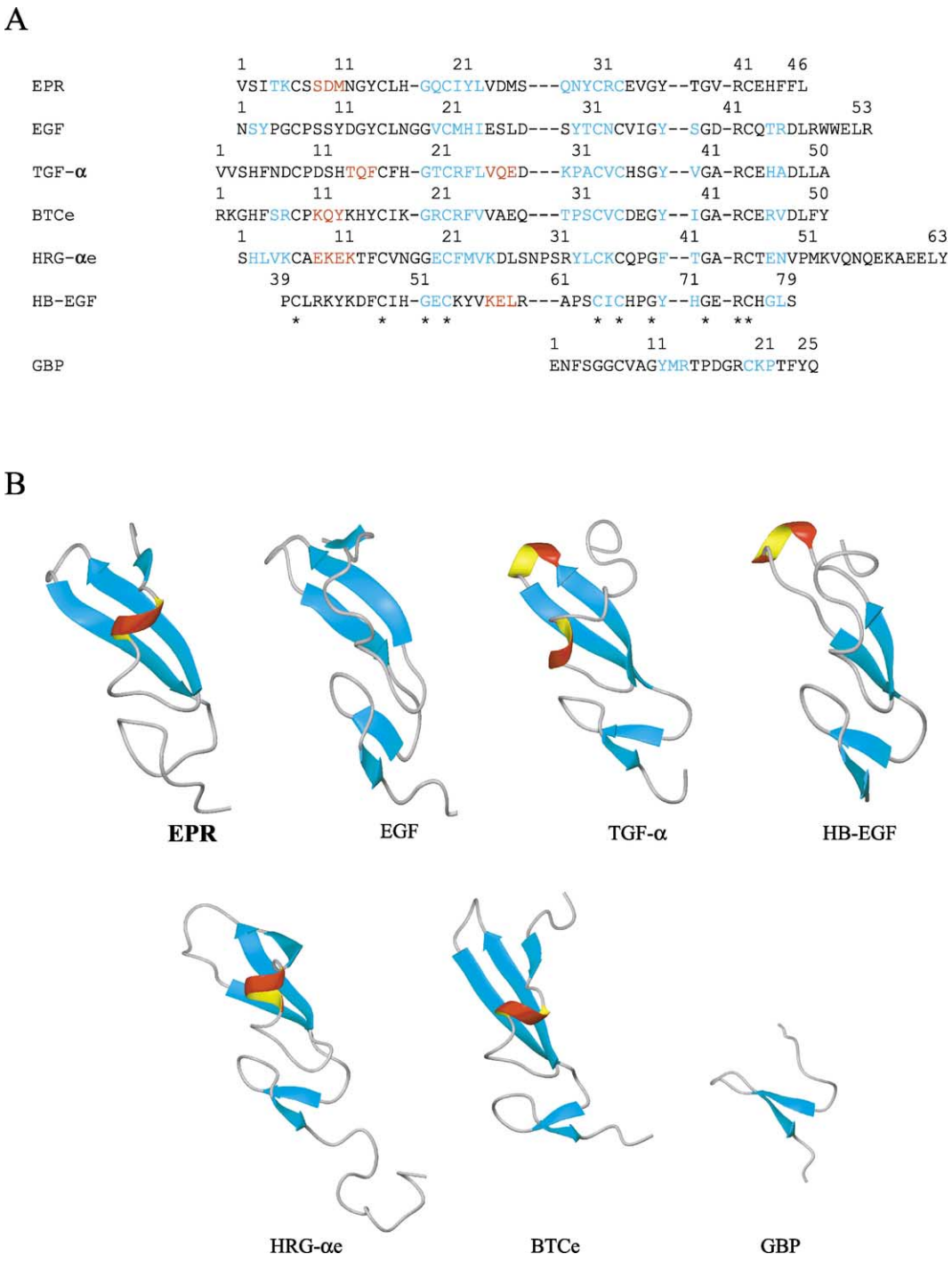

Fig. 3. Sequence alignment and comparisons of the secondary structure of EGF-family ligands including EPR (A) and comparisons of tertiary structures of EGF-family ligands and EPR (B). The numbers in panel A are residue numbers in the amino acid sequence of each protein. The asterisks indicate the conserved residues of ligands, except for GBP. In the alignment, the blue characters indicate β-sheet regions and the red characters indicate helical regions. The drawing of EGF-family ligands and GBP was made using atomic coordinates obtained from the PDB, and the accession codes are 1EGF [13], 2TGF [14], 1HAF [15], 1IOX [16], 1XDT [17], and 1BQF [37] for EGF, TGF-α, HRG-αe, BTCe, HB-EGF, and GBP, respectively. The model structures were generated using the program MOLMOL [30].

short helical turn (Ser^{8}-Met^{10}). The β-sheet structure consisting of strand-1, -2, and -3 is arranged in an antiparallel manner. The atomic coordinates for the final structures of EPR were deposited in the PDB (PDB accession code is 1K36 for the 40 ensemble structures and 1K37 for the energy-minimized average structure).

3.3. The structure of the N-terminal domain of EPR

The comparisons of the secondary and tertiary structures between EPR and other EGF-family proteins are shown in Fig. 3A,B. The secondary and tertiary structures of the N-terminal domain of EPR are similar to those of other EGF-family proteins. Comparing EPR, EGF, TGF-α, BTCe,

A

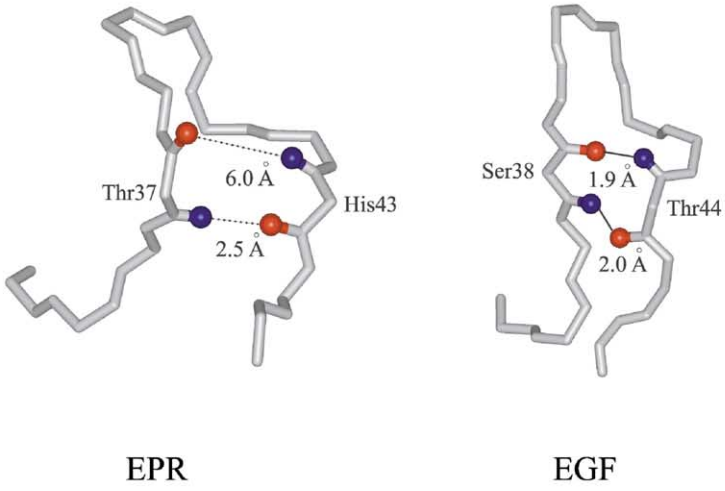

B

	Residue	Atom	Residue	Atom	Length (Å)
EPR	Thr^{37}	NH	His^{43}	O	2.54
	His^{43}	NH	Thr^{37}	O	5.97
EGF	Ser^{38}	NH	Thr^{44}	O	1.95
	Thr^{44}	NH	Ser^{38}	O	1.94
TGF-α	Val^{39}	NH	His^{45}	O	1.71
	His^{45}	NH	Val^{39}	O	2.06
BTCe	Ile^{39}	NH	Arg^{45}	O	1.86
	Arg^{45}	NH	Ile^{39}	O	2.20
HRG-αe	Thr^{41}	NH	Gly^{47}	O	1.91
	Gly^{47}	NH	Thr^{41}	O	2.20

Fig. 4. A: Comparison of the structure in the C-terminal domain between EPR and EGF. Hydrogen bonds between Ser^{38} and Thr^{44} in EGF are shown by continuous lines with the hydrogen bond lengths. The lengths between backbone NH and O atoms in EPR are shown by dotted lines. Backbone NH and O atoms are represented by blue and red, respectively. B: Comparison of the hydrogen bond lengths (Å) in the C-terminal domain among EGF-family ligands. The lengths between backbone NH and O atoms in EPR are shown for comparison.

HRG-αe, and HB-EGF, we found a common structural property in the β-sheet that consists of strand-2 and -3, corresponding to Gly^{17}-Leu^{22} and Gln^{27}-Cys^{32} of EPR, and the short turn structure between the two strands (Fig. 3A). In addition, the tertiary structure of this region of EPR is similar to the corresponding regions of other ligands (Fig. 3B). Another interesting similarity between EPR and other EGF-family ligands is that EPR, BTCe, and HRG-αe adopt a helical turn in this region of Ser^{8}-Met^{10} in EPR (Fig. 3A). Tertiary structures of this region are similar to each other among these three proteins (Fig. 3B). EGF, TGF-α, and HB-EGF do not form the helical turn in this region. In particular, the structures in the N-terminal domain are similar between EPR and BTCe, which are the ligands for ErbB-1 and ErbB-4 [10–12].

3.4. The structure of the C-terminal domain of EPR

Although the overall structure of the N-terminal domain of EPR is similar to those of other EGF-family ligands, there is a marked difference in the structure of the C-terminal domain between EPR and other EGF-family ligands. The C-terminal portions of EGF, TGF-α, BTCe, HRG-αe, and HB-EGF form an antiparallel β-sheet. However, the C-terminal portion of EPR does not form a complete β-sheet structure (Figs. 2 and 3). Montelione et al. [13] have reported the H–D exchange rate of backbone amide protons of EGF. The back-

bone amide protons of Tyr[37], Ser[38], Cys[42], Gln[43] and Thr[44] of EGF exchanged slowly with deuterium in the H–D exchange experiment and the interstrand NOEs were observed in the C-terminal β-sheet of EGF [39]. Only one slowly exchanging amide proton was observed in the C-terminal domain of EPR in the amide H–D exchange experiment (Fig. 1) and there was no NOE between two segments (Tyr[36]-Thr[37] and His[43]-Phe[44]) in the C-terminal domain of EPR (data not shown). These results suggest that conformation in this region of EPR is not supported by hydrogen bonds and that the lack of hydrogen bonds is responsible for the incomplete β-sheet structure in the C-terminal domain of EPR. However, the C-terminal domain adopts a β-sheet-like structure according to $^{3}J_{NH\alpha H}$ and CSI analysis (Fig. 1). Therefore, EPR slightly differs from other EGF-like ligands in the conformation of the C-terminal domain.

Although EPR is a ligand that binds to the homodimer of ErbB-1 and ErbB-4 and the heterodimer containing ErbB-2, the binding affinity of EPR is much lower than those of other EGF-family ligands [1,11,31]. Structural differences between EPR and other EGF-family ligands may be associated with the low binding affinity of EPR for the receptors. The importance of the structure in the C-terminal domain of EGF-family ligands has been suggested in several studies [18–20]. The C-terminal domain includes Arg[41], Asp[42], and Leu[47] of human EGF, and Arg[42] of human TGF-α; these residues are responsible for optimal association with the ErbB-1 receptor [32–35]. Recently, the crystal structure of the extracellular domains of ErbB-1 bound to EGF has been reported. The region containing the loop (residues 6–9) and Arg41 of EGF interacts with site 2 in domain III of ErbB-1, and the C-terminal region around Arg45 of EGF interacts with site 3 in domain III of ErbB-1 [41]. The crystal structure of the complex of TGF-α and ErbB-1 extracellular domain has also been determined, showing that a number of residues in the C-terminal domain of TGF-α interact with the extracellular domain of ErbB-1 [42]. In addition, the HRG-α and HRG-β isoforms are identical in the EGF domain sequence up to fifth Cys, and both directly bind ErbB-3 and ErbB-4, although their binding affinities are significantly different. The binding of HRG-α is 100-fold weaker than that of HRG-β for the ErbB-3 and ErbB-4 homodimers [11]. An insect cytokine, growth-blocking peptide (GBP) has an overall fold similar to the C-terminal domain of EGF, even though GBP lacks the N-terminal domain [37] (Fig. 3B). A previous study has shown that GBP directly binds and activates the EGF receptor in keratinocyte cells and enhances cell proliferation of human keratinocyte cells with a potency almost equivalent to that of human EGF [36]. Therefore, the C-terminal domain may play an important role in binding of EGF-like ligands to ErbB receptors, and so the difference in the ligand–receptor binding affinity may depend on structural differences in the C-terminal domain.

The C-terminal domains of EGF, TGF-α, BTCe, HRG-αe, and HB-EGF have a short turn and a continuing double-stranded β-sheet, and GBP has a similar conformation with the C-terminal domain of EGF. On the other hand, EPR does not form a complete β-sheet structure in the C-terminal domain (Figs. 1–3). Fig. 4 shows the comparison of structures in the C-terminal domain among EGF-family ligands. In the C-terminal domain of EGF, hydrogen bonds are formed between the Ser[38] and Thr[44] [39] (Fig. 4A). These hydrogen bonds also exist in the C-terminal domain of TGF-α, HRG-αe and BTCe (Fig. 4B). However, the corresponding residues of EPR, Thr[37] and His[43], do not form the hydrogen bonds (Fig. 4A). The incomplete β-sheet structure in the C-terminal domain of EPR results from the fact that only the amide proton of Thr[37] exchanges slowly in the H–D exchange experiment and the lack of the interstrand NOEs between two segments (Tyr[36]-Thr[37] and His[43]-Phe[44]) in the C-terminal domain (Fig. 1). The structures of EGF, TGF-α, HRG-αe, BTCe and GBP previously reported were determined by NMR and these structures, except for TGF-α, were solved at acidic pH (pH 2.0–4.5) [13–16,37,40]. We analyzed the NOESY spectrum of EPR at pH 7.0 and confirmed that there was no interstrand NOEs in the C-terminal domain of EPR at pH 7.0. The far-UV CD spectra show that the conformation of EPR does not change in the pH range of 3.4–7.0 (Fig. 5). The far-UV CD mainly reflects the secondary structure of proteins and is slightly contributed by aromatic side chains and disulfide bonds. The similarity of the structures at pH 3.4 and 7.0 is also evident from the CSI data, which depend on the secondary structure of proteins [27]. Moreover, a previous NMR study has shown that the structures of EGF at pH 6.8 and 2.0 are nearly identical except for the region of Asp[46]-Arg[53] [40]. Therefore, the lack of β-sheet structure in the C-terminal domain of EPR at pH 3.4 is not due to the low pH. The structural difference in the C-terminal domain may provide an explanation for the reduced binding affinity of EPR to the ErbB receptors.

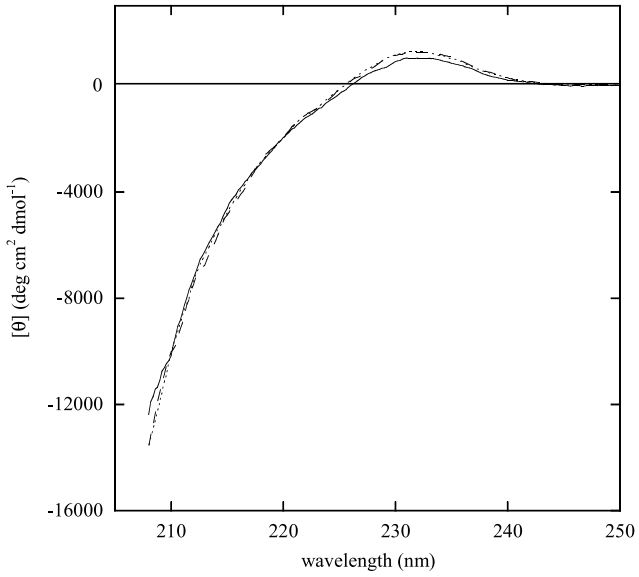

Fig. 5. CD spectra of EPR in the far-UV region at various pHs. Continuous, dotted and dashed lines represent the spectra of EPR at pH 3.4, 6.0 and 7.0, respectively.

Acknowledgements: This work was supported by grants from the Program for the Promotion of Basic Research Activities for Innovative Biosciences (PROBRAIN) and from the Ministry of Education, Culture, Sports, Science and Technology of Japan to K.K.

References

[1] Toyoda, H., Komurasaki, T., Uchida, D., Takayama, Y., Isobe, T., Okuyama, T. and Hanada, K. (1995) J. Biol. Chem. 270, 7495–7500.

[2] Toyoda, H., Komurasaki, T., Ikeda, Y., Yoshimoto, M. and Morimoto, S. (1995) FEBS Lett. 377, 403–407.
[3] Toyoda, H., Komurasaki, T., Uchida, D. and Morimoto, S. (1997) Biochem. J. 326, 69–75.
[4] Sasaki, E., Arakawa, T., Fujiwara, Y., Kawada, N., Fukuda, T., Higuchi, K., Komurasaki, T. and Kobayashi, K. (1997) Eur. J. Pharmacol. 338, 253–258.
[5] Shirakata, Y., Komurasaki, T., Toyoda, H., Hanakawa, Y., Yamasaki, K., Tokumaru, S., Sayama, K. and Hashimoto, K. (2000) J. Biol. Chem. 275, 5748–5753.
[6] Hashimoto, K. (2000) J. Dermatol. Sci. 24, S46–S50.
[7] Zhu, Z., Kleeff, J., Friess, H., Wang, L., Zimmermann, A., Yarden, Y., Buchler, M.W. and Korc, M. (2000) Biochem. Biophys. Res. Commun. 273, 1019–1024.
[8] Baba, I., Shirasawa, S., Iwamoto, R., Okumura, K., Tsunoda, T., Nishioka, M., Fukuyama, K., Yamamoto, K., Mekada, E. and Sasazuki, T. (2000) Cancer Res. 60, 6886–6889.
[9] van der Geer, P., Hunter, T. and Lindberg, R.A. (1994) Annu. Rev. Cell Biol. 10, 251–337.
[10] Komurasaki, T., Toyoda, H., Uchida, D. and Morimoto, S. (1997) Oncogene 15, 2841–2848.
[11] Jones, J.T., Akita, R.W. and Sliwkowski, M.X. (1999) FEBS Lett. 447, 227–231.
[12] Riese II, D.J., Komurasaki, T., Plowman, G.D. and Stern, D.F. (1998) J. Biol. Chem. 273, 11288–11294.
[13] Montelione, G.T., Wüthrich, K., Burgess, A.W., Nice, E.C., Wagner, G., Gibson, K.D. and Scheraga, H.A. (1992) Biochemistry 31, 236–249.
[14] Harvey, T.S., Wilkinson, A.J., Tappin, M.J., Cooke, R.M. and Campbell, I.D. (1991) Eur. J. Biochem. 198, 555–562.
[15] Jacobsen, N.E., Abadi, N., Sliwkowski, M.X., Reilly, D., Skelton, N.J. and Fairbrother, W.J. (1996) Biochemistry 35, 3402–3417.
[16] Miura, K., Doura, H., Aizawa, T., Tada, H., Seno, M., Yamada, H. and Kawano, K. (2002) Biochem. Biophys. Res. Commun. 294, 1040–1046.
[17] Louie, G.V., Yang, W., Bowman, M.E. and Choe, S. (1997) Mol. Cell 1, 67–78.
[18] Engler, D.A., Montelione, G.T. and Niyogi, S.K. (1990) FEBS Lett. 271, 47–50.
[19] Dudgeon, T.J., Cooke, R.M., Baron, M., Campbell, I.D., Edwards, R.M. and Fallon, A. (1990) FEBS Lett. 261, 392–396.
[20] Kramer, R.H., Lenferink, A.E., van Bueren-Koornneef, I.L., van der Meer, A., van de Poll, M.L. and van Zoelen, E.J. (1994) J. Biol. Chem. 269, 8708–8711.
[21] Seno, M., Tada, H., Kosaka, M., Sasada, R., Igarashi, K., Shing, Y., Folkman, J., Ueda, M. and Yamada, H. (1996) Growth Factors 13, 181–191.
[22] Rance, M., Sørensen, O.W., Bodenhausen, G., Wagner, G., Ernst, R.R. and Wüthrich, K. (1983) Biochem. Biophys. Res. Commun. 117, 479–485.
[23] Braunschweiler, L. and Ernst, R.R. (1983) J. Magn. Reson. 53, 521–528.
[24] Jeener, J., Meier, B.H., Bachmann, P. and Ernst, R.R. (1979) J. Chem. Phys. 71, 4546–4553.
[25] Delaglio, F., Grzesiek, S., Vuister, G.W., Zhu, G., Pfeifer, J. and Bax, A. (1995) J. Biomol. NMR 6, 277–293.
[26] Garrett, D.S., Powers, R., Gronenborn, A.M. and Clore, G.M. (1991) J. Magn. Reson. 95, 214–220.
[27] Wishart, D.S., Sykes, B.D. and Richards, F.M. (1992) Biochemistry 31, 1647–1651.
[28] Brünger, A.T. (1992) X-PLOR Manual, Version 3.1, Yale University Press, Cambridge, MA.
[29] Koradi, R., Billeter, M. and Wüthrich, K. (1996) J. Mol. Graph. 14, 51–55.
[30] Wüthrich, K. (1986) in: NMR of Proteins and Nucleic Acids, Wiley-Interscience, New York.
[31] Shelly, M., Pinkas-Kramarski, R., Guarino, B.C., Waterman, H., Wang, L.M., Lyass, L., Alimandi, M., Kuo, A., Bacus, S.S., Pierce, J.H., Andrews, G.C. and Yarden, Y. (1998) J. Biol. Chem. 273, 10496–10505.
[32] Matsunami, R.K., Campion, S.R., Niyogi, S.K. and Stevans, A. (1990) FEBS Lett. 264, 105–108.
[33] Engler, D.A., Campion, S.R., Hauser, M.R., Cook, J.S. and Niyogi, S.K. (1992) J. Biol. Chem. 267, 2274–2281.
[34] Defeo-Jones, D., Tai, J.Y., Vuocolo, G.A., Wegrzyn, R.J., Schofield, T.L., Riemen, M.W. and Oliff, A. (1989) Mol. Cell. Biol. 9, 4083–4086.
[35] Puddicombe, S.M., Chamberlin, S.G., MacGarvie, J., Richter, A., Drummond, D.R., Collins, J., Wood, L. and Davies, D.E. (1996) J. Biol. Chem. 271, 15367–15372.
[36] Ohnishi, A., Oda, Y. and Hayakawa, Y. (2001) J. Biol. Chem. 276, 37974–37979.
[37] Aizawa, T., Fujitani, N., Hayakawa, Y., Ohnishi, A., Ohkubo, T., Kumaki, Y., Kawano, K., Hikichi, K. and Nitta, K. (1999) J. Biol. Chem. 274, 1887–1890.
[38] Laskowski, R.A., Rullmannn, J.A., MacArthur, M.W., Kaptein, R. and Thornton, J.M. (1996) J. Biomol. NMR 8, 477–486.
[39] Montelione, G.T., Wuthrich, K., Nice, E.C., Burgess, A.W. and Scheraga, H.A. (1986) Proc. Natl. Acad. Sci. USA 83, 8594–8598.
[40] Kohda, D. and Inagaki, F. (1992) Biochemistry 31, 11928–11939.
[41] Ogiso, H., Ishitani, R., Nureki, O., Fukai, S., Yamanaka, M., Kim, J.H., Saito, K., Sakamoto, A., Inoue, M., Shirouzu, M. and Yokoyama, S. (2002) Cell 110, 775–787.
[42] Garrett, T.P., McKern, N.M., Lou, M., Elleman, T.C., Adams, T.E., Lovrecz, G.O., Zhu, H.J., Walker, F., Frenkel, M.J., Hoyne, P.A., Jorissen, R.N., Nice, E.C., Burgess, A.W. and Ward, C.W. (2002) Cell 110, 763–773.